Findings across pre-clinical models in the development of PT-112, a novel investigational platinum-pyrophosphate anti-cancer agent

T. Ames[1], B. Slusher[2], K. Wozniak[2], W. Kerns[3], K.L. Fong[3], P. Pourquier[4], C. Gongora[4], J. Jimeno[1], D. Chatterjee[5].

[1]Phosplatin Therapeutics, Clinical and Translational Research and Development, New York, USA. [2]Johns Hopkins University School of Medicine, Johns Hopkins Drug Discovery and Department of Neurology, Baltimore, USA. [3]Accellient Partners, Toxicology and Pharmacokinetics, Waltham, USA. [4]Institut de Recherche en Cancérologie de Montpellier, Cellular Biology, Montpellier, France. [5]Rhode Island Hospital and The Alpert Medical School of Brown University, Department of Medicine, Providence, USA.

Acknowledgments: Phosplatin Therapeutics gratefully acknowledges the contributions of Y. Takase, H. Shimizu, K. Nishibata-Kobayashi, and R.M. Kanada-Sonobe of Eisai & Co., Ltd. Discovery Chemistry, Tsukuba, Japan.

PHOSPLATIN THERAPEUTICS

Background

PT-112 is a new chemical entity under clinical development in the US and Taiwan, designed to minimize particular toxicities associated with traditional platinum agents and drug resistance stemming from DNA damage and repair. As a pyrophosphate-conjugated Pt-containing anti-neoplastic therapeutic, PT-112 differs from platinum therapies in both mechanism and toxicity. In previous work in cancer cell models, PT-112 exposure resulted in significantly less Pt accumulation in both DNA and whole cell extracts compared with exposure to either cisplatin (cis) or oxaliplatin (oxali). Nonetheless, PT-112 has potent cytotoxic activity in *in vitro* systems, implying a different spectrum of targets for PT-112 in comparison to traditional platinum compounds. In this work, we explore the activity and mechanism of action of PT-112 by investigating impacts on cancer related proteins and pathways, including those connected to immunogenic cell death (ICD), as well as how PT-112 potency is affected by DNA repair pathways. Lastly, PT-112 anticancer activity, pharmacokinetics (PK), and toxicity are measured in multiple *in vivo* systems.

Results

In vitro experiments revealed unique features of PT-112 in both activity and mechanism. Specifically, IC_{50} values for PT-112 were superior to cis, carboplatin (carbo), and oxali in a majority of cell lines, in a broadly platinum-resistant cell panel. A high degree of correlation was observed between cis and carbo activity, but not between those agents and PT-112. A correlation between PT-112 and oxali was also observed, and led to investigation of cellular targets and mechanisms not shared by these two agents. In an HCT116 colon cancer model, PT-112 had a minimal effect on the phosphorylation of H2AX and on induction of Ku70 versus oxali at equipotent concentrations, implying PT-112 has a low degree of reliance on DNA-binding and damage for anti-cancer activity. Additionally, PT-112's potency did not differ significantly between nucleotide excision repair (NER)-deficient HCT116 cells and their isogenic NER-proficient counterparts. Conversely, NER-competent cells were less sensitive to cis treatment versus the NER-deficient cell line. PT-112 also had a noteworthy impact on p53 and MDM2 levels, in addition to numerous proteins involved in inhibition of cell cycle progression at the G1/S phase, such as p16 and p21 and downstream members of the CDK and E2F families. PT-112 also induced a variety of effects indicative of ICD induction at a significantly greater extent than oxali, which is considered a *bona fide* ICD-inducing agent. These effects comprise the release of HMGB1, cell surface exposure of calreticulin (CRT), and suppression of STAT3.

In vivo experiments demonstrated the activity of PT-112 as a single agent across multiple tumor models, as well as pronounced differences in pharmacokinetics and toxicity relative to other platinum compounds. Specifically, in the GXF97 gastric patient-derived xenograft (PDX) model, a durable response was observed (minimum $\Delta T/\Delta C$ = 2.5%) at 90 mg/kg. Cases of complete response were observed, albeit at higher doses not tolerated by all other mice in those cohorts (data not shown). Sustained tumor growth delay was observed with PT-112 treatment in the CXF280 colon PDX and PANC1 pancreatic cancer models.

PK experiments in rats demonstrated a large fraction of PT-112-derived Pt in the plasma ultrafiltrate (PUF) relative to total plasma Pt (72.8%), notably contrasting with data from the literature using oxali, where a much smaller fraction of Pt in the PUF was observed (28.2%). Importantly, Pt in plasma, but not present in the PUF, is believed to be protein-bound and not bioavailable for therapeutic benefit. An LC-MS/MS analytical method developed to detect parent PT-112 also revealed its predominance, indicating stability of PT-112 in plasma (data not shown).

Rats tolerated 7-fold higher concentrations of PT-112 with minimal effects on renal function (creatinine, BUN and GFR) versus cis, which caused morbidity. In a mouse model of acute neurotoxicity, a single dose of PT-112 was indistinguishable from untreated controls when given at twice the molar concentration of oxali, which induced a significant increase in cold hypersensitivity. After repeat doses over 4 weeks to test for indicators of chronic neuropathy, PT-112 caused minimal accumulation of Pt in dorsal root ganglia (DRG) nerve tissue and no significant loss in nerve conduction velocity (NCV), while oxali treatment caused both dose-dependent declines in NCV and significantly greater Pt accumulation in DRG. Reductions in NCV are indicative of chronic neuropathy and have been shown to be caused by DRG Pt accumulation.

Conclusions

PT-112 bears the hallmarks of a highly differentiated, pleiotropic and well-tolerated anti-cancer agent. Specifically, PT-112: (1) works effectively in both *in vitro* and *in vivo* cancer models; (2) is minimally impacted by DNA repair pathways, suggesting DNA is not the primary target; (3) acts in part through the p53/MDM2 pathway, along with G1/S cell cycle regulators; (4) induces the hallmarks of ICD; (5) is stable in plasma; (6) results in negligible renal toxicity relative to cis at significantly higher doses; and (7) produces no measurable signs of acute or chronic neuropathy in contrast to oxali. Additionally, the concentrations used herein relate to PT-112 plasma levels achievable in human patients at sub-toxic doses. These findings suggest that PT-112 represents a clinically relevant departure from the paradigm associated with approved Pt agents. Further translational research is underway, in parallel with an ongoing Phase I clinical study at the MD Anderson Cancer Center, the Sarah Cannon Research Institute, the University of Colorado Cancer Center, and the Mayo Clinic Cancer Center.

Chemical Structure

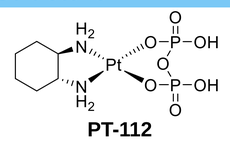

PT-112

Figure 1: Chemical structure of PT-112

In Vitro Activity

Cell Line	Cell Type	IC_{50} Values (μM) cis	carbo	oxali	PT-112
HCT116	Colorectal	>10	>10	2.7	3.8
HMV-1	Cervical, Adenoca.	>10	>10	6.3	3.6
COV362	Ovarian, Endometroid	12.4	34.9	17.1	>10
EFO-21	Ovarian, Adenoca.	32.2	>50	7.2	>10
OV56	Ovarian, Serous	2.6	13.5	3.9	4.4
OVCAR4	Ovarian, Adenoca.	7.6	21.1	2.9	2.7
A427	Lung	4.7	12.6	1.5	0.9
Calu6	Lung, Anaplastic Ca.	0.9	2.3	0.2	0.1
HCC827	Lung, EGFRmut	14.8	39.9	0.8	0.5
NCI-H1703	Lung, Squamous	13.3	15.2	2	1.1
NCI-H226	Lung, Squamous	9.1	17.4	1.9	1.1
A2058	Skin, Melanoma	7.4	>10	11.5	8.1
MeWo	Skin, Melanoma	13.5	27.5	6.8	4.9
RPMI7951	Skin, Melanoma	3.2	7.9	5	2.2
SK-MEL-28	Skin, Melanoma	34.7	>50	19.8	7.8

Figure 2: Comparative *in vitro* activity of cisplatin, carboplatin, oxaliplatin, and PT-112. Cells were exposed to different concentrations of drug over 72 hours, and the number of surviving cells were measured via WST-8 assay. In cases where a definitive IC_{50} was determined for PT-112, it was the most active in a majority of cell lines.

DNA Damage and Repair

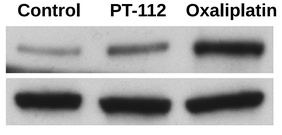

Figure 3: H2AX phosphorylation. Above is a western blot analysis of HCT116 cells treated with IC_{50} concentrations of PT-112 or oxali for 48h. Enhanced levels of phosphorylated H2AX (pH2AX) indicate the presence of DNA damage and repair.

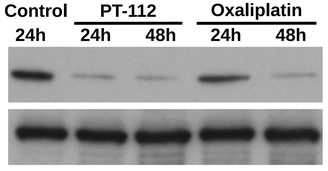

Figure 4: Ku70 expression. Western blot analysis of HCT116 cells treated with IC_{50} concentrations of PT-112 and oxali for 48h, above. Elevated levels of Ku70 are indicative of activation of the non-homologous end joining DNA repair pathway.

DNA Damage and Repair, Continued

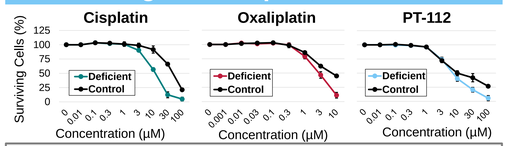

Figure 5: DNA Repair Impact on Drug Sensitivity. The sensitivity to cis, oxali, and PT-112 was measured in a series of cell line pairs, comprising a parental and a modified cell line, in which the XPD protein essential to NER was knocked out. Significant differences in the survival curves above imply an impact of the NER pathway on drug sensitivity and resistance. Error bars indicate +/-1 SEM.

Tumor Suppressor Pathway Activity

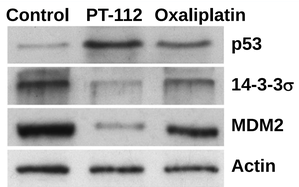

Figure 6: p53 Pathway Modulation. Above is a western blot analysis of p53, MDM2, and 14-3-3σ expression in HCT116 cells treated with IC_{50} concentrations of PT-112 or oxali for 24h. Induction of p53 could be explained by reduction in MDM2. Notably stronger effects on the expression of these proteins as well as on 14-3-3σ were observed in the PT-112 vs oxali-treated cells.

Cell Cycle Arrest

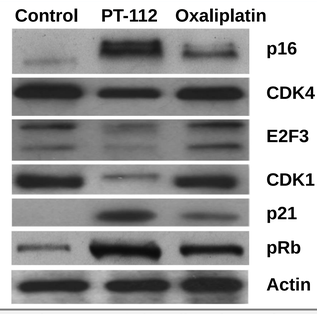

Figure 7: Drug impact on G1/S cell cycle regulators. Western blot analysis of HCT116 cells treated with IC_{50} concentrations of PT-112 and oxali for 48h, above. Relative to oxali and control, decreased levels of CDK1, CDK4, and E2F3 in addition to elevated levels of p16, p21, and pRb expression were observed in cells treated with PT-112.

Immunogenic Cell Death†

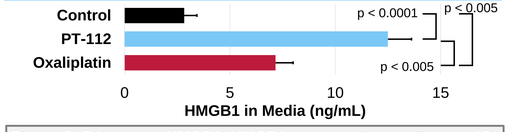

Figure 8: Release of HMGB1. HMGB1 in the media of cells after 48h of drug treatment was measured via ELISA. HMGB1 release is involved in ICD and antigen presentation to dendritic cells. Error bars indicate 1 SEM, and p-values were generated using two-tailed t-tests.

Immunogenic Cell Death, Continued†

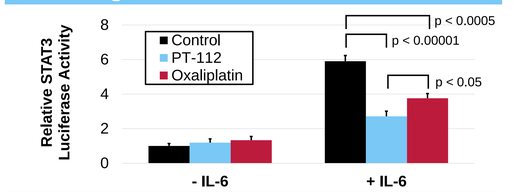

Figure 9: Inhibition of STAT3 transcriptional activity. HCT116 cells were transfected with an IRF-1 reporter plasmid for STAT3 transcriptional luciferase reporter activity. After 48h, cells were exposed to IL-6 (in order to induce STAT3) and each agent as indicated for 24h. STAT3 activity represses ICD. Two experiments repeated in quadruplicate are averaged and normalized to the IL-6 negative control samples. Error bars indicate 1 SEM, and p-values were generated using two-tailed t-tests.

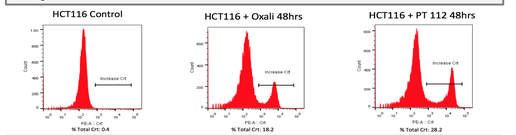

Figure 10: Cell Surface Expression of Calreticulin. CRT cell surface expression was measured via flow cytometry after 48h of drug treatment. A peak present to the right of the main peak indicates cells staining positive for CRT, a hallmark of ICD and an inducer of phagocyte targeting.

†Adapted from Wang et al., 2015 AACR-NCI-EORTC Conference Poster Abstract C32

In Vivo Activity

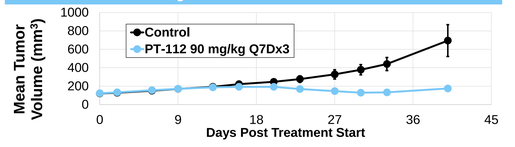

Figure 11: GXF97 PDX Gastric Cancer Xenograft. Mice were implanted with tumor tissue and randomized into control or treatment groups (n=6). Points represent the average tumor size for a particular group/time. Minimum $\Delta T/\Delta C$ was 2.5%. Error bars represent +/- 1 SEM.

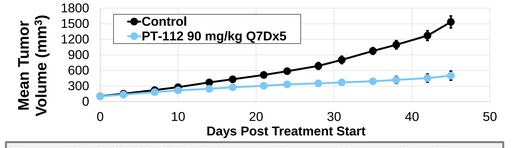

Figure 12: CXF280 PDX Colorectal Cancer Xenograft. Mice were implanted with tumor tissue and randomized into control or treatment groups (n=6). Points represent average tumor sizes for a particular group/time. Minimum $\Delta T/\Delta C$ was 28%. Error bars represent +/- 1 SEM.

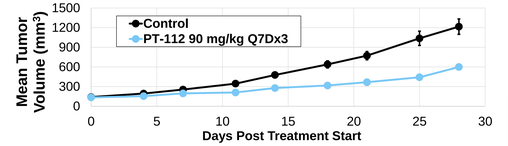

Figure 13: PANC1 Pancreatic Cancer Xenograft. Mice were implanted with tumor cells and randomized into control (n=10) or treatment groups (n=5). Points represent average tumor sizes for each group/time. Minimum $\Delta T/\Delta C$ was 34%. Error bars represent +/- 1 SEM.

Pharmacokinetics

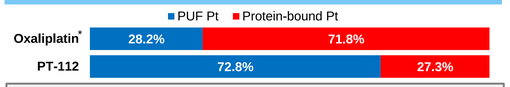

Figure 14: Ratio of Protein-Bound vs. Unbound Pt in Rat Plasma. Pt (measured by ICP-MS) was measured both in plasma and PUF. The amount of Pt in the PUF is represented by the blue bar, whereas the red bar represents Pt in plasma not accounted for by PUF Pt (i.e. plasma protein-bound) and unlikely to be bioavailable for therapeutic benefit. Data for PT-112 represent averages from 4 treated animals.
*Luo et al., *Cancer Chemother Pharmacol* 44, 1999.

Toxicology

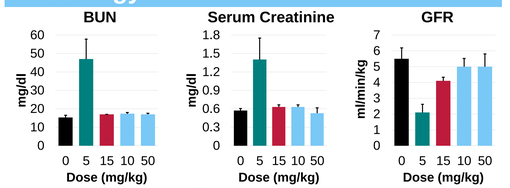

Figure 15: Renal Toxicology. Rats were dosed with single injections of the indicated agent. After 4 days, blood and urine were collected, BUN and serum creatinine were measured, and GFR was calculated. Height of bars represent the average measurements and calculations, and error bars show 1 SEM.

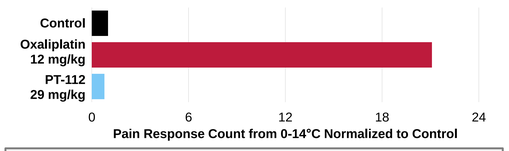

Figure 16: Acute Neuropathy. Mice were treated with vehicle (n=8), oxali (n=8), or PT-112 (n=9). PT-112 was dosed at twice the molar concentration of oxali. At 92-96h post dosing, mice were placed on a temperature-controlled surface set to 30°C. The temperature was then reduced by 1°C/min down to 0°C, and signs of pain and discomfort were quantified. Oxali treatment provoked significant cold hyperalgesia, whereas PT-112 treatment was indistinguishable from control.

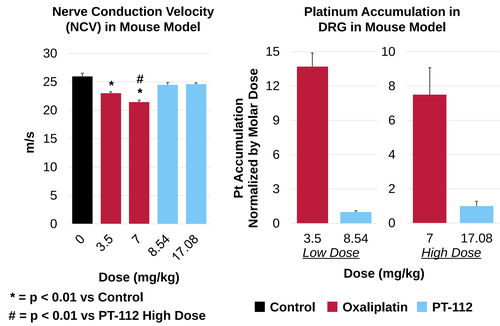

Figure 17: Chronic Neuropathy. Groups of 10 mice were treated with 8 (low dose experiments) or 7 (high dose experiments) doses of oxali or PT-112 over a 4 week period. NCVs were measured before treatment (data not shown), where no meaningful differences in the groups were detected, and after treatment. Subsequently, in a subset of the mice (n=4-5 per group) DRG tissue was removed, and Pt content was measured using established methods via ICP-MS.